purification. ^{13}C NMR: δ 19.4, 20.1, 23.6, 24.3, 24.9, 25.4, 26.8, 42.3, 44.8, 50.8, 54.8, 58.2, 125.9, 126.4, 144.2, 146.6, 157.6, 159.0, 180.6.

2,3,10,11,13,19-Hexamethyl-23-[2-(1-methylpyridiniumyl)]-3,10,14,18,21,25-hexaazabicyclo[10.7.7]hexacosa-1,11,13,18,20,25-hexaene hexafluorophosphate (13a), 2,3,9,10,12,18-hexamethyl-22-[2-(1-methylpyridiniumyl)]-3,9,13,17,20,24-hexaazatricyclo[9.7.7]pentacosa-1,10,12,17,20,24-hexaene hexafluorophosphate (13b), and 2,3,11,12,14,20-hexamethyl-24-(2-pyridyl)-3,11,15,19,22,26-hexaazatricyclo[11.7.7.1^{5,9}]octacosa-1,5,7,9(28),12,14,19,21,26-nonaene hexafluorophosphate (13c) were prepared in the manner described for **14a**. **(2,3,10,11,13,19-Hexamethyl-23-[2-(1-methylpyridiniumyl)]-3,10,14,18,21,25-hexaazabicyclo[10.7.7]hexacosa-1,11,13,18,20,25-hexaene-κ^4*N*)cobalt(II) Hexafluorophosphate (15a).** A solution of **13a** (0.28 g, 0.25 mmol) in methanol (15 mL) was heated at reflux, and a warm solution of sodium acetate (0.034 g, 0.41 mmol) and cobalt(II) acetate (0.125 g, 0.71 mmol) was added. The dark orange solution was heated at reflux for a further 30 min. Upon cooling, a yellow precipitate was obtained that was collected by filtration, rinsed with diethyl ether, and then dried under vacuum. Yield: 0.2 g (78%). Anal. Calcd for $C_{32}H_{50}N_7P_3F_{18}Co$: C, 37.44; H, 4.91; N, 9.55; Co, 5.74; P, 9.05. Found (two determinations): C, 37.40 (37.56); H, 4.86 (5.06); N, 9.68 (9.35); Co, 5.61 (5.61); P, ... (8.99).

(2,3,10,11,13,19-Hexamethyl-23-(2-pyridyl)-3,10,14,18,21,25-hexaazabicyclo[10.7.7]hexacosa-1,11,13,18,20,25-hexaene-κ^4*N*)cobalt(II) Hexafluorophosphate (16a). Methanol (15 mL) containing **14a** (0.16 g, 0.14 mmol) was heated at reflux, and methanol (10 mL) containing cobalt(II) acetate (0.05 g, 0.28 mmol) and sodium acetate (0.01 g, 0.14 mmol) was added. The orange solution was heated at reflux for 20 min and allowed to cool to room temperature. A deep red solid was collected by filtration and then dried under vacuum. ESR spectroscopy indicates that this fraction corresponds to the pure exo isomer. Yield: 0.03 g (24%). Further concentration of the solution resulted in the isolation of isomer mixtures containing predominantly the endo isomer. Yield: 0.05 g (45%). Elemental analyses were performed on both fractions. Anal. Calcd for $C_{31}H_{47}N_7P_2F_{12}Co$: C, 42.96; H, 5.46; N, 11.31; P, 7.15; Co, 6.80. Found: C, 42.94 (42.70); H, 5.46 (5.43); N, 11.31 (11.41); P, 7.17 (...); Co, 6.73 (6.89).

Crystal Structure Analysis of Complex 11a. Crystal data: $C_{32}H_5I_3N_7Ni\cdot H_2O$, M_r = 990.2, orthorhombic, *Pna*2$_1$, a = 12.247 (2) Å, b = 25.236 (6) Å, c = 12.260 (2) Å, V = 3789 (1) Å^3, Z = 4, D_c = 1.74 g cm^{-3}, D_m = 1.61 g cm^{-3}, λ = 0.71069 Å, μ(Mo Kα) = 29.6, T = 20 °C. An isomerically pure sample of compound **10a** was obtained by repeated careful fractional crystallization until purity was confirmed by extended-time FT ^{13}C NMR spectroscopy. The isomerically pure sample was then metathesized to compound **11a**, the iodide salt. Irregular orange-red needles were obtained by slow evaporation of an aqueous solution of **11a**. Data were collected with a Syntex $P2_1$ four circle diffractometer. The maximum 2θ was 50°, with a scan range of ±0.85° (2θ) around the $K\alpha_1$-$K\alpha_2$ angles and scan speed of 2-29° min^{-1}, depending on the intensity of a 2-s prescan; backgrounds were measured at each end of the scan for 0.25 of the scan time. Three standard reflections were monitored every 200 reflections and showed a slight decrease during data collection; the data were rescaled to correct for this. Density was measured by flotation. Unit cell dimensions and standard deviations were obtained by least-squares fit to 15 reflections. All 3534 unique reflections ($I/\sigma(I) \geq 2.5$) were used in refinement; they were corrected for Lorentz, polarization, and absorption effects, the last by the analytical method; maximum and minimum transmission factors were 0.68 and 0.54. Crystal dimensions were 0.50 × 1.1 × 0.50 mm.

Systematic absences $0kl$ ($k + l = 2n + 1$) and $h0l$ ($h = 2n + 1$) indicated either the space group *Pna*2$_1$ or *Pnam* (nonstandard). Statistical analysis suggested the former, which was shown to be correct by successful refinement. Positions for the three I atoms and one Ni atom were assigned from a Patterson synthesis and the light atoms then found on successive Fourier syntheses (including solvent H_2O). In the final refinement, a weighting scheme

$$w = 1.0/(1 + ((F_o - 60)/25)^2)$$

was used with all hydrogen atom positions (except those on the water molecule) calculated with fixed isotropic temperature factors and all non-hydrogen atoms refined anisotropically. The Z coordinate of I(1) was held fixed to define the origin. The final R values were R = 0.056 and R_w = 0.063. A final difference Fourier map had no electron density areas greater than 0.5 electron in magnitude, indicating that all electron density had been reasonably assigned. Computing was with X-ray 72. Scattering factors and anomalous dispersion factors were taken from ref 35. Final atomic coordinates are given in Table II. Structure factors are given in ref 25.

Acknowledgment. Support of this research by the National Science Foundation, Grant No. CHE-8402153, and the National Institutes of Health, Grant No. GM 10040, is gratefully acknowledged. The Ohio State University and the University of Warwick collaboration has been supported by a NATO travel grant.

Supplementary Material Available: Table S1 (full bond lengths and angles) and Table S2 (anisotropic thermal parameters and H atom coordinates) (5 pages); Table S3 (structure factors) (24 pages). Ordering information is given on any current masthead page.

(35) *International Tables for X-ray Crystallography*; Kynoch Press: Birmingham, England, 1974.

Contribution from the Department of Chemistry and Biochemistry, University of Notre Dame, Notre Dame, Indiana 46556, and Department of Physics, The Pennsylvania State University, University Park, Pennsylvania 16802

Axial Ligand Orientation in Iron(II) Porphyrinates. Preparation and Characterization of Low-Spin Bis(imidazole)(tetraphenylporphyrinato)iron(II) Complexes

Martin K. Safo,[1] W. Robert Scheidt,*[,1] and Govind P. Gupta*[,2]

Received July 11, 1989

The preparation of several low-spin bis(1-substituted imidazole)(tetraphenylporphyrinato)iron(II) complexes is reported (1-substituted imidazole = 1-vinylimidazole, 1-benzylimidazole, 1-methylimidazole, 1-acetylimidazole, and 1-(trimethylsilyl)imidazole). These complexes have been characterized by Mössbauer and UV-vis spectroscopy. The Mössbauer isomer shifts are in the range 0.43-0.47 mm s^{-1} and the quadrupole splittings are in the range 0.97-1.07 mm s^{-1}. The crystal and molecular structure of two of these complexes has been determined by single-crystal X-ray diffraction studies. The two complexes, [Fe(TPP)(1-VinIm)$_2$] and [Fe(TPP)(1-BzlIm)$_2$], have crystallographically imposed inversion centers that lead to parallel ligand plane orientations. Comparisons of the molecular structures of these two species with those of several analogous iron(III) derivatives reveals similar trends in the orientation of the axial imidazole ligands. However, the iron(II) derivatives do show larger axial imidazole "tilts" and "tips". The average Fe-N_p distances are 2.001 (2) Å for [Fe(TPP)(1-VinIm)$_2$] and 1.993 (9) Å for [Fe(TPP)(1-BzlIm)$_2$]; Fe-N(Im) bond distances are 2.004 (2) Å for [Fe(TPP)(1-VinIm)$_2$] and 2.017 (4) Å for [Fe(TPP)(1-BzlIm)$_2$]. Crystal data for [Fe(TPP)(1-VinIm)$_2$]·CH_2Cl_2: monoclinic, $FeCl_2N_8C_{55}H_{42}$, a = 18.871 (4) Å, b = 11.644 (3) Å, c = 22.766 (5) Å, β = 112.90 (1)°, V = 4613.2 Å^3, Z = 4, space group $C2/c$, 4756 observed unique data, all measurements at 293 K. Crystal data for [Fe(TPP)(1-BzlIm)$_2$]: triclinic, $FeN_8C_{64}H_{48}$, a = 10.952 (5) Å, b = 11.402 (5) Å, c = 10.803 (9) Å, α = 104.02 (6)°, β = 105.24 (6)°, γ = 97.65 (4)°, V = 1234.6 Å^3, Z = 1, space group $P\bar{1}$, 3496 observed unique data, all measurements at 118 K.

In hemoproteins, a most interesting physicochemical problem is the wide variation of their physical properties; even those hemoproteins having the same set of heme substituents and the same axial ligands can display remarkably diverse properties.[3] We have

0020-1669/90/1329-0626$02.50/0

been concerned with understanding possible structural bases for controlling differing physical properties. We have been particularly concerned with the factors that affect redox potentials, electronic ground states, and the electronic and magnetic resonance spectra. One important factor for controlling and modulating the above properties has been identified in these laboratories: a combination of X-ray crystal structure determinations and physical property measurements has shown that the axial ligand orientation in iron(III) porphyrinates can control (i) the apparent ground state of complexes and (ii) both major and minor variations in the electron paramagnetic resonance spectra. Thus, distinct electronic ground states for different crystalline forms of $[Fe(OEP)(3\text{-}Cl\text{-}py)_2]ClO_4$[5,6] can be correlated with changes in ligand orientation angle (ϕ).[7] In this pyridine-ligated species, the form[9] with a large value of orientation angle (near 45°) has a low-spin–high-spin thermal equilibrium spin state, while the forms[10,11] with small values of ϕ have quantum admixed intermediate-spin states. Different crystalline forms of [Fe(TPP)(NCS)(py)] with differing magnetic properties are also consistent with the concept of axial ligand orientation control of spin state.[12,13]

We have also found that the relative axial ligand orientation ($\Delta\phi$) has significant effects on EPR spectra. Perpendicular alignment ($\Delta\phi \approx 90°$) of axial ligand planes produces species displaying an unusual low-spin EPR signal, the so-called strong g_{max} signal.[4,14,15] Two different studies show that bis(imidazole) complexes with parallel relative imidazole ligand orientations ($\Delta\phi = 0°$) have "normal" rhombic EPR spectra but the precise g values are exquisitely sensitive to the orientation angle ϕ.[16,17] Walker et al.[4,18] have suggested that perpendicular relative orientations of two axial imidazole ligands (compared to a parallel orientation) could affect the redox potential by approximately 50 mV. Thus ligand orientation effects could provide a means of fine-tuning the redox potential of cytochromes *b*.

Imidazole, in the form of a histidine residue, is a very important axial ligand in hemoproteins. Histidines are found to provide one or two axial ligands in most hemoproteins. Despite the prevalence of imidazole ligation in hemes, very little structural information on imidazole coordination is available for iron(II) species. In particular, given the information described above for iron(III) complexes, it would be useful to understand if there are significant differences in ligand orientation preference for iron(II) compared to iron(III) porphyrinates. In this paper, we report the preparation and spectroscopic characterization (Mössbauer, UV–vis, IR) of five bis(imidazole)iron(II) porphyrinates. We have also determined the molecular structures of two of these species and compare them, in detail, with the analogous iron(III) complexes.

Table I. Summary of Crystal Data and Intensity Collection Parameters

	$[Fe(TPP)(1\text{-}VinIm)_2]\cdot CH_2Cl_2$	$[Fe(TPP)(1\text{-}BzlIm)_2]$
formula	$FeCl_2N_8C_{55}H_{42}$	$FeN_8C_{64}N_{48}$
fw	941.74	985.0
space group	$C2/c$	$P\bar{1}$
T, K	293	118
a, Å	18.871 (4)	10.952 (8)
b, Å	11.644 (3)	11.402 (5)
c, Å	22.766 (5)	10.803 (9)
α, deg	90.0	104.02 (6)
β, deg	112.90 (1)	105.24 (6)
γ, deg	90.0	97.65 (4)
V, Å^3	4613.19	1234.60
D(obsd), g/cm^3	1.35	1.30
D(calcd), g/cm^3	1.36	1.31
no. of obsd data	4756	3496
R_1	0.047	0.070
R_2	0.049	0.076

Experimental Section

General Information. All solvents were distilled under argon prior to use. Benzene was distilled from sodium benzophenone ketyl. Dichloromethane and hexane were distilled from CaH_2. 1-Vinylimidazole, 1-benzylimidazole, 1-acetylimidazole, 1-(trimethylsilyl)imidazole, 1-methylimidazole, and ethanethiol were obtained from Aldrich and used without further purification. All procedures were carried out under argon by general Schlenk and cannula techniques. $Fe^{II}TPP$ was prepared by reduction of $[Fe(TPP)_2O]$ with ethanethiol.[19] $Fe^{II}TPP$ samples are best handled in the drybox when finely divided in order to avoid oxidation. Samples for Mössbauer spectroscopy were prepared in an inert-atmosphere glovebox as Apiezon L grease mulls or wax suspensions (melting point 78 °C). Mössbauer measurements were made at 4.2 and/or 77 K, and in some cases with an applied magnetic field. UV–vis spectra were recorded on a Perkin-Elmer Lambda 4C spectrometer, and IR spectra, on a Perkin-Elmer 883 spectrometer.

Synthesis of [Fe(TPP)(1-VinIm)$_2$]. $[Fe(TPP)(1\text{-}VinIm)_2]$ was prepared by reacting Fe(TPP) (200 mg, 0.299 mmol) with 1-vinylimidazole (572 mg, 6.10 mmol) in 30 mL of dichloromethane. The solution was warmed slightly with stirring for 10 min and then filtered. The filtrate was layered with about 60 mL of hexane by cannulation and the Schlenk flask set in the freezer (−16 °C) for crystallization. X-ray diffraction quality crystals formed after 3 days. Yield: 252 mg, 98.4%. IR (KBr): 1649 cm^{-1} (C=C, imidazole). UV–vis (CH_2Cl_2) λ_{max}, nm (log ϵ): 423.9 (5.22), 533.2 (4.24), 564.2 (3.67).

Synthesis of [Fe(TPP)(1-BzlIm)$_2$]. This was prepared as above, with Fe(TPP) (200 mg, 0.299 mmol) and 1-benzylimidazole (480 mg, 2.99 mmol). Diffraction quality crystals formed after 2 days. Yield: 220 mg, 74.5%. UV–vis (CH_2Cl_2) λ_{max}, nm (log ϵ): 426.3 (5.23), 533.2 (4.19), 565.3 (3.63).

Synthesis of [Fe(TPP)(1-AcIm)$_2$]. This was prepared as above, with Fe(TPP) (100 mg, 0.150 mmol) and 1-acetylimidazole (248 mg, 2.20 mmol). Needlelike crystals formed after 2 days. IR (KBr): 1746 cm^{-1} (C=O, imidazole). UV–vis (CH_2Cl_2) λ_{max}, nm (log ϵ): 422.4 (5.14), 532.7 (3.99), 563.2 (3.62).

Synthesis of [Fe(TPP)(1-Me$_3$SiIm)$_2$]. This was prepared with Fe(TPP) (200 mg, 0.299 mmol) and 1-(trimethylsilyl)imidazole (750 mg, 5.30 mmol) in 30 mL of THF, with slight warming and stirring for 10 min.

(1) University of Notre Dame.
(2) The Pennsylvania State University.
(3) In a previous paper[4] we have detailed some of the observed hemoprotein property variations for species having bis(histidine) ligation (cytochromes *b*).
(4) Walker, F. A.; Huynh, B. H.; Scheidt, W. R.; Osvath, S. R. *J. Am. Chem. Soc.* **1986**, *108*, 5288–5297.
(5) Three crystalline forms of $[Fe(OEP)(3\text{-}Cl\text{-}py)_2]ClO_4$ have been isolated and characterized. One form, *tri*-$[Fe(OEP)(3\text{-}Cl\text{-}py)_2]ClO_4$, was found to have a thermal spin equilibrium state ($S = {}^5/_2$, $S = {}^1/_2$), while the other two forms, *mono*-$[Fe(OEP)(3\text{-}Cl\text{-}py)_2]ClO_4$ and $[Fe(OEP)(3\text{-}Cl\text{-}py)_2]ClO_4\cdot CHCl_3$, were found to have admixed intermediate-spin states. See refs 9–11.
(6) Abbreviations used in this paper: TPP, OEP, and Prot IX, the dianions of *meso*-tetraphenylporphyrin, octaethylporphyrin, and protoporphyrin IX, respectively; 1-MeIm, 1-methylimidazole; 1-VinIm, 1-vinylimidazole; 1-BzlIm, 1-benzylimidazole; 1-AcIm, 1-acetylimidazole; 1-Me$_3$SiIm, 1-(trimethylsilyl)imidazole; HIm, imidazole; 3-Cl-py, 3-chloropyridine; py, pyridine; *c*-MU and *t*-MU, *cis*- and *trans*-methyl urocanate (methyl 4-imidazoleacrylate) respectively; N_p, porphinato nitrogen; N_4, plane of the four porphinato nitrogen atoms; THF, tetrahydrofuran.
(7) We follow the original suggestion of Hoard et al.[8] for defining this orientation angle as the dihedral angle between the axial ligand plane and a coordinate plane defined by a porphinato nitrogen atom, the metal atom, and the donor atom of the coordinated axial ligand. The symbol ϕ is typically used for this orientation angle.
(8) Collins, D. M.; Countryman, R.; Hoard, J. L. *J. Am. Chem. Soc.* **1972**, *94*, 2066–2072.
(9) Scheidt, W. R.; Geiger, D. K.; Haller, K. J. *J. Am. Chem. Soc.* **1982**, *104*, 495–499.
(10) Scheidt, W. R.; Geiger, D. K.; Lee, Y. J.; Reed, C. A.; Lang, G. *Inorg. Chem.* **1987**, *26*, 1039–1045.
(11) Scheidt, W. R.; Geiger, D. K.; Hayes, R. G.; Lang, G. *J. Am. Chem. Soc.* **1983**, *105*, 2625–2632.
(12) Geiger, D. K.; Chunplang, V.; Scheidt, W. R. *Inorg. Chem.* **1985**, *24*, 4736–4741.
(13) Scheidt, W. R.; Lee, Y. J.; Geiger, D. K.; Taylor, K.; Hatano, K. *J. Am. Chem. Soc.* **1982**, *104*, 3367–3374.
(14) Scheidt, W. R.; Kirner, J. F.; Hoard, J. L.; Reed, C. A. *J. Am. Chem. Soc.* **1987**, *109*, 1963–1968.
(15) Inniss, D.; Soltis, S. M.; Strouse, C. E. *J. Am. Chem. Soc.* **1988**, *110*, 5644–5650.
(16) Scheidt, W. R.; Osvath, S. R.; Lee, Y. J. *J. Am. Chem. Soc.* **1987**, *109*, 1958–1963.
(17) Soltis, S. M.; Strouse, C. E. *J. Am. Chem. Soc.* **1988**, *110*, 2824–2829.
(18) See ref 4 for other references concerning the possible effects of axial ligand orientation on redox potential in hemoproteins.
(19) Stolzenberg, A. M.; Strauss, S. H.; Holm, R. H. *J. Am. Chem. Soc.* **1981**, *103*, 4763–4778.

Table II. Fractional Coordinates for $[Fe(TPP)(1\text{-VinIm})_2]\cdot CH_2Cl_2$[a]

atom	x	y	z
Fe	0.7500	0.2500	0.5000
Cl(1)	0.03441 (8)	0.09948 (13)	−0.29572 (5)
N(1)	0.80854 (9)	0.19708 (15)	0.44817 (7)
N(2)	0.65664 (9)	0.16824 (14)	0.44028 (7)
N(3)	0.78920 (9)	0.11152 (15)	0.55553 (8)
N(4)	0.85426 (10)	−0.04699 (16)	0.59833 (8)
C(a1)	0.88600 (11)	0.21239 (18)	0.46233 (9)
C(a2)	0.78195 (11)	0.12957 (18)	0.39404 (9)
C(a3)	0.64874 (11)	0.10783 (18)	0.38591 (9)
C(a4)	0.58405 (11)	0.17038 (18)	0.44147 (9)
C(b1)	0.90751 (12)	0.15232 (20)	0.41653 (10)
C(b2)	0.84370 (12)	0.10259 (20)	0.37430 (10)
C(b3)	0.57034 (12)	0.07039 (21)	0.35343 (10)
C(b4)	0.53074 (12)	0.10875 (21)	0.38731 (11)
C(m1)	0.70668 (11)	0.08988 (18)	0.36330 (10)
C(m2)	0.56337 (11)	0.22638 (17)	0.48645 (10)
C(11)	0.47967 (11)	0.22195 (18)	0.47713 (10)
C(12)	0.45195 (13)	0.13534 (20)	0.50378 (12)
C(13)	0.37364 (14)	0.12819 (23)	0.49170 (14)
C(14)	0.32363 (13)	0.20917 (26)	0.45380 (14)
C(15)	0.35082 (14)	0.29699 (26)	0.42852 (13)
C(16)	0.42881 (13)	0.30379 (23)	0.44022 (12)
C(21)	0.68711 (11)	0.02641 (20)	0.30176 (10)
C(22)	0.68665 (13)	0.08439 (23)	0.24804 (11)
C(23)	0.66867 (15)	0.02647 (29)	0.19081 (12)
C(24)	0.65099 (15)	−0.0880 (3)	0.18634 (13)
C(25)	0.65094 (16)	−0.14596 (26)	0.23857 (14)
C(26)	0.66913 (14)	−0.08873 (23)	0.29632 (12)
C(1)	0.79017 (15)	0.09525 (22)	0.61585 (12)
C(2)	0.82923 (15)	−0.00083 (23)	0.64217 (11)
C(3)	0.82775 (12)	0.02398 (20)	0.54684 (10)
C(4)	0.89987 (14)	−0.14508 (22)	0.60409 (12)
C(5)	0.93664 (17)	−0.20114 (27)	0.65662 (15)
C(6)	0.0000	0.1847 (5)	−0.2500

[a] The estimated standard deviations of the least significant digits are given in parentheses.

The product precipitated, and hexane (50 mL) was added to effect complete precipitation. The precipitate was filtered out and dried under vacuum. Yield: 150 mg, 52.6%. IR (KBr): 2919, 701 cm^{-1} (CH_3 and Si–C, imidazole). UV-vis (CH_2Cl_2) λ_{max}, nm: 420.4, 536.2, 564.5, 589.2.

Synthesis of [Fe(TPP)(1-MeIm)$_2$]. This was prepared as described for $[Fe(TPP)(1\text{-}Me_3SiIm)_2]$ with Fe(TPP) (100 mg, 0.150 mmol) and 1-methylimidazole (125 mg, 1.52 mmol). Yield: 96 mg, 77.2%. UV-vis (CH_2Cl_2) λ_{max}, nm CH_2Cl_2 (log ϵ): 424.6 (5.09), 533.5 (4.26), 564.4 (3.75).

Structure and Determinations

[Fe(TPP)(1-VinIm)$_2$]. A rectangular crystal of $[Fe(TPP)(1\text{-VinIm})_2]$ examined on a Syntex $P\bar{1}$ diffractometer was established as a four-molecule monoclinic unit cell with space group *Cc* or *C2/c*. Least-squares refinement of 60 automatically centered reflections with $21.10 < 2\theta < 29.30°$ led to the cell constants reported in Table I. Intensity data for $[Fe(TPP)(1\text{-VinIm})_2]$ were measured as described in Table I and Table IS (supplementary material). Four standard reflections were measured; there was no decay of intensity during data collection. Intensity data were reduced with the profile-fitting algorithm of Blessing.[20] All data with $F_o \geq 3.0\sigma(F_o)$ were retained as observed and used in all subsequent least-squares refinements. The structure was solved by using the direct methods program MULTAN78.[21] The centrosymetric space group was assumed, and all subsequent developments of structure solution and refinement were consistent with this choice. Difference Fourier syntheses led to the location of all hydrogen atoms in the structure. The hydrogen atoms were idealized and included in subsequent cycles of least-squares refinements as fixed contributors (C–H = 0.95 Å, $B(H) = B(C) + 1.0$ Å^2). Least-squares refinement converged smoothly. The highest peak in the final difference Fourier map was 0.285 e/Å^3, and the map was judged featureless. Final atomic coordinates are listed in Table II. Final anisotropic temperature factors and hydrogen atom positions are given in Tables IIS and IIIS (supplementary material).

Table III. Fractional Coordinates for $[Fe(TPP)(1\text{-BzlIm})_2]$[a]

atom	x	y	z
Fe(1)	0.0000	0.0000	0.0000
N(1)	0.1705 (4)	−0.0111 (3)	0.1168 (4)
N(2)	−0.0406 (3)	0.0885 (3)	0.1618 (4)
N(3)	0.0698 (4)	0.1667 (3)	−0.0160 (4)
N(4)	0.0939 (4)	0.3103 (3)	−0.1178 (4)
C(a1)	0.2580 (4)	−0.0751 (4)	0.0769 (4)
C(a2)	0.2190 (4)	0.0338 (4)	0.2534 (4)
C(a3)	0.0372 (4)	0.1238 (4)	0.2935 (4)
C(a4)	−0.1461 (4)	0.1415 (4)	0.1660 (4)
C(b1)	0.3643 (4)	−0.0699 (4)	0.1926 (5)
C(b2)	0.3413 (4)	−0.0029 (4)	0.3002 (5)
C(b3)	−0.0226 (4)	0.1956 (4)	0.3800 (4)
C(b4)	−0.1356 (5)	0.2078 (4)	0.3008 (5)
C(m1)	0.2483 (4)	−0.1369 (4)	−0.0536 (5)
C(m2)	0.1594 (4)	0.0972 (4)	0.3383 (4)
C(1)	0.1028 (5)	0.2819 (4)	0.0771 (5)
C(2)	0.1156 (5)	0.3702 (4)	0.0146 (5)
C(3)	0.0662 (5)	0.1885 (4)	−0.1319 (5)
C(4)	0.0865 (5)	0.3646 (4)	−0.2287 (5)
C(5)	−0.0476 (5)	0.3809 (4)	−0.2953 (5)
C(6)	−0.1593 (5)	0.3035 (5)	−0.3008 (6)
C(7)	−0.2807 (5)	0.3171 (6)	−0.3703 (7)
C(8)	−0.2893 (6)	0.4094 (6)	−0.4338 (7)
C(9)	−0.1791 (6)	0.4869 (6)	−0.4276 (6)
C(10)	−0.0594 (5)	0.4730 (4)	−0.3587 (5)
C(11)	0.3476 (4)	−0.2102 (4)	−0.0775 (4)
C(12)	0.4515 (5)	−0.1652 (5)	−0.1158 (5)
C(13)	0.5387 (5)	−0.2378 (5)	−0.1423 (6)
C(14)	0.5230 (5)	−0.3577 (5)	−0.1325 (5)
C(15)	0.4198 (5)	−0.4035 (4)	−0.0952 (5)
C(16)	0.3342 (5)	−0.3304 (4)	−0.0663 (5)
C(17)	0.2305 (4)	0.1408 (4)	0.4852 (4)
C(18)	0.2060 (5)	0.0696 (4)	0.5679 (5)
C(19)	0.2735 (5)	0.1080 (5)	0.7049 (5)
C(20)	0.3634 (5)	0.2183 (5)	0.7593 (5)
C(21)	0.3887 (5)	0.2890 (5)	0.6779 (5)
C(22)	0.3235 (5)	0.2497 (4)	0.5411 (5)

[a] The estimated standard deviations of the least significant digits are given in parentheses.

[Fe(TPP)(1-BzlIm)$_2$]. A preliminary examination of a rectangular crystal of this complex on an Enraf-Nonius CAD4 diffractometer led to a one-molecule triclinic cell. Least-squares refinement of 25 automatically centered reflections gave the cell constants reported in Table I. Three standard reflections were measured; there was no decay of intensity during the data collection. Data reduction and structure solution were as above. Hydrogen atoms were idealized as before. Least-squares refinement converged smoothly. The highest peak in the final difference Fourier map is 1.1 e/Å^3, near the iron atom. The final map was judged otherwise to display no significant features. Final atomic coordinates are listed in Table III. Crystal data and intensity collection parameters for the complex are found in Tables I and IS. Final anisotropic temperature factors and fixed hydrogen atom positions are given in Tables IVS and VS of the supplementary material.

Results

Both IR and UV–vis spectroscopies were used to identify and ascertain the oxidation states of the complexes. IR spectra confirm the presence of bound vinylimidazole (C=C, 1649 cm^{-1}), acetylimidazole (C=O, 1746 cm^{-1}), and (trimethylsilyl)imidazole (CH_3, 2919 cm^{-1}; Si—C, 701 cm^{-1}) ligands. More importantly, the IR spectra do not show peaks at 890 and 870 cm^{-1}, which are characteristic of μ-oxo iron(III) complex formation.[22,23] The UV–vis spectral bands at 420–427 nm and 532–537 nm, with a

(20) Blessing, R. H. *Crystallogr. Rev.* **1987**, *1*, 3–58.
(21) Programs used in this study included local modifications of Main, Hull, Lessinger, Germain, Declerq, and Woolfson's MULTAN78, Jacobson's ALLS, Zalkin's FORDAP, Busing and Levy's ORFFE, and Johnson's ORTEP2. Atomic form factors were from: Cromer, D. T.; Mann, J. B. *Acta Crystallogr., Sect. A* **1968**, *A24*, 321–323. Real and imaginary corrections for anomalous dispersion in the form factor of the iron atom were from: Cromer, D. T.; Liberman, D. J. *J. Chem. Phys.* **1970**, *53*, 1891–1898. Scattering factors for hydrogen were from: Stewart, R. F.; Davidson, E. R.; Simpson, W. T. *Ibid* **1965**, *42*, 3175–3187. All calculations were performed on a VAX 11/730.
(22) Reed, C. A.; Mashiko, T.; Scheidt, W. R.; Spartalian, K.; Lang, G. *J. Am. Chem. Soc.* **1980**, *102*, 2302–2306.
(23) Hoffman, A. B.; Collins, D. M.; Day, V. W.; Fleisher, E. B.; Srivastava, T. S.; Hoard, J. L. *J. Am. Chem. Soc.* **1972**, *94*, 3620–3626.

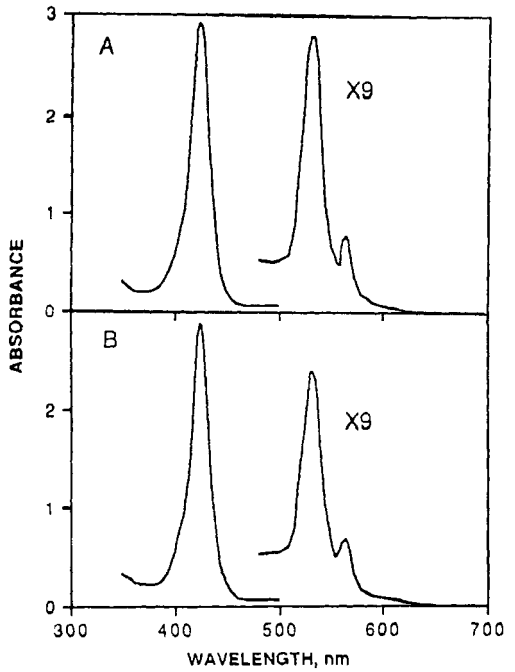

Figure 1. UV–vis spectra of 1.75×10^{-4} M solution of [Fe(TPP)(1-VinIm)$_2$] (A) and 1.69×10^{-4} M solution of [Fe(TPP)(1-BzlIm)$_2$] (B).

Table IV. Mössbauer Data for (1-Substituted imidazole)$_2$Fe^{II}(TPP) Complexes[a]

complex	T, K	δ, mm s^{-1}	ΔE, mm s^{-1}	line width, mm s^{-1}
[Fe(TPP)(1-VinIm)$_2$]	77	0.45	1.02	0.23
	4.2	0.43	1.00	0.26
	4.2 (6 T)[b]	0.46	1.02	0.23
[Fe(TPP)(1-SiMe$_3$Im)$_2$]	77	0.46	1.04	0.23
	4.2	0.46	1.03	0.23
	4.2 (6 T)[b]	0.46	1.03	0.23
[Fe(TPP)(1-BzlIm)$_2$]	77	0.45	1.02	0.23
[Fe(TPP)(1-AcIm)$_2$]	77	0.45	0.97	0.22
[Fe(TPP)1-MeIm)$_2$]	77	0.47	1.07	0.25

[a] Isomer shifts are relative to metallic iron. [b] Applied magnetid field of 6 T.

characteristic shoulder at 562–566 nm, are typical of other low-spin iron(II) tetraphenylporphyrinates[24] and confirm the Fe(II) oxidation state. The UV–vis spectra of 1-vinylimidazole and 1-benzylimidazole derviatives, which are typical of all complexes, are shown in Figure 1. Thus both the IR and UV–vis characterizations are consistent with all complexes being formulated as low-spin bis(imidazole)-ligated Fe(II) derivatives.

Mössbauer spectra of all complexes have also been obtained, and parameters are given in Table IV. In the absence of an applied magnetic field at 77 K, the spectra of the five complexes show similar isomer shifts (δ) of 0.43–0.47 mm s^{-1} and quadrupole splittings (ΔE) of 0.97–1.07 mm s^{-1}. Typical spectra are shown in Figure 2. These values are similar to others reported[25,26] and are characteristic of low-spin Fe(II) porphyrinates. Two complexes, [Fe(TPP)(1-VinIm)$_2$] and [Fe(TPP)(1-Me$_3$SiIm)$_2$], were studied at 77 and 4.2 K; the Mössbauer parameters are insensitive to temperature. The Mössbauer spectra of the vinylimidazole and the (trimethylsilyl)imidazole complexes were also obtained in the presence of an applied magnetic field, and double-doublet spectra are observed (Figure 2). Analysis of magnetic spectra confirms the diamagnetic nature of these iron(II) species and provides a

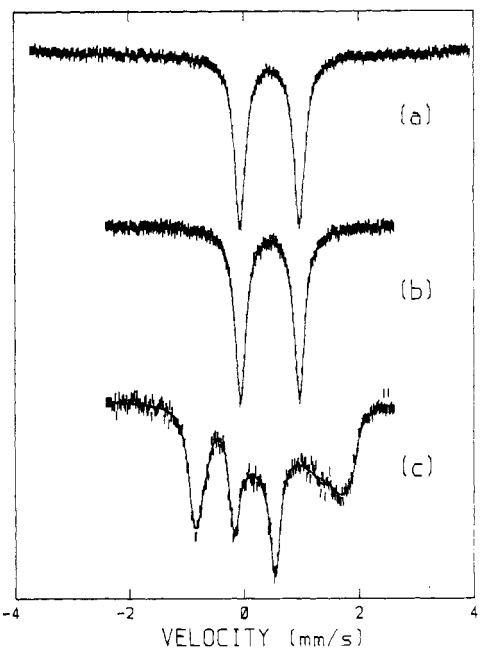

Figure 2. Mössbauer spectra of [Fe(TPP)(1-Me$_3$SiIm)$_2$] at 77 (a) and 4.2 K (b) in the absence of an applied magnetic field and in the presence of an applied 6 T magnetic field (c).

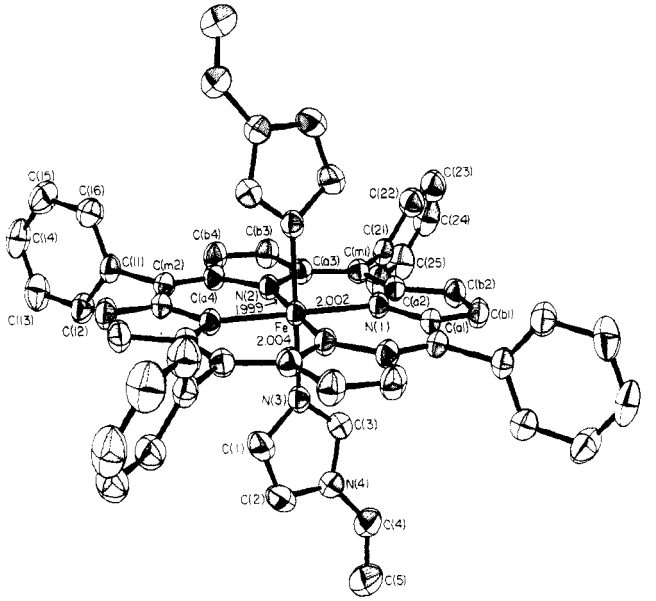

Figure 3. ORTEP diagram of the [Fe(TPP)(1-VinIm)$_2$] molecule. Labels assigned to the crystallographically unique half of the centrosymmetric molecule are displayed. Bond distances in the coordination group are shown.

positive sign of the quadrupole splitting with an asymmetry parameter $\eta = 0$.[27]

We have determined the molecular structure of two of the five complexes, [Fe(TPP)(1-VinIm)$_2$] and [Fe(TPP)(1-BzlIm)$_2$]. The structure of a third complex, [Fe(TPP)(1-MeIm)$_2$, has been solved by Hoard et al. and briefly reported.[28] Overall views of the molecular structures of [Fe(TPP)(1-VinIm)$_2$] and [Fe(TPP)(1-BzlIm)$_2$] are given in Figures 3 and 4. The numbering scheme and bond distances in the coordination group are also displayed in these figures. Both complexes have crystallographically required

(24) Collman, J. P.; Brauman, J. I.; Doxsee, K. M.; Halbert, T. R.; Bunnenberg, E.; Linder, R. E.; LaMar, G. N.; Gaudio, J. D.; Lang, G.; Spartalian, K. *J. Am. Chem. Soc.* **1980**, *102*, 4182–4192.
(25) Dolphin, D.; Sams, J. R.; Tsin, T. B.; Wong, K. L. *J. Am. Chem. Soc.* **1976**, *98*, 6970–6975.
(26) Epstein, L. M.; Straub, D. K.; Maricondi, C. *Inorg. Chem.* **1967**, *6*, 1720–1724.
(27) Greenwood, N. N.; Gibb, T. C. *Mössbauer Spectroscopy*; Chapman and Hall Ltd.: London, 1971; pp 54–59.
(28) (a) Steffen, W. L.; Chun, H. K.; Hoard, J. L.; Reed, C. A. *Abstracts of Papers*, 175th National Meeting of the American Chemical Society, Anaheim, CA; March, 13–17, 1978; American Chemical Society: Washington, DC, 1978; INOR 15. (b) Hoard, J. L. Personal communication.

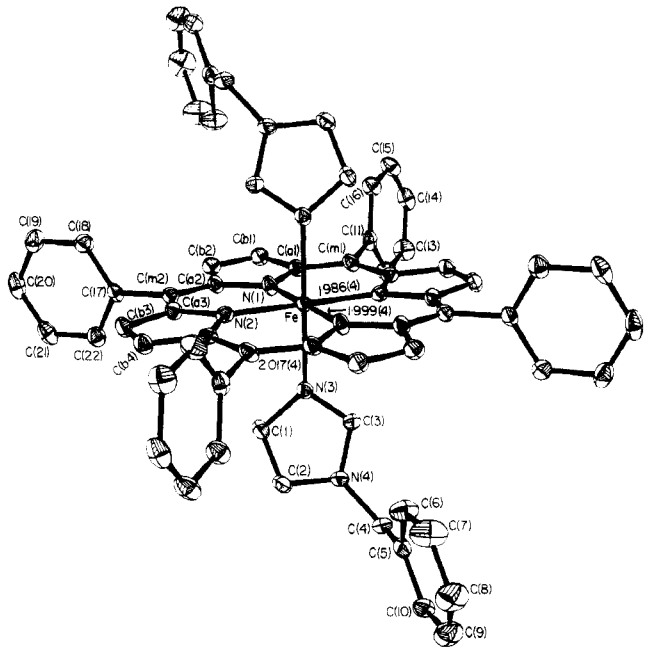

Figure 4. ORTEP diagram of the centrosymmetric $[Fe(TPP)(1\text{-BzlIm})_2]$ molecule. Same information as Figure 3 is given.

Table V. Summary of Fe–N Bond Distances in Bis(imidazole)iron(II) and -(III) Complexes[a]

complex	Fe–N_p[b]	Fe–N(Im)[b]	(Fe–N)[b,d]	ref
	A. Iron(II) Complexes			
$[Fe(TPP)(1\text{-VinIm})_2]$	2.001 (2)	2.004 (2)	2.002	this work
$[Fe(TPP)(1\text{-BzlIm})_2]$	1.993 (9)	2.017 (4)	2.001	this work
$[Fe(TPP)(1\text{-MeIm})_2]$	1.997 (6)	2.014 (5)	2.002	28b
	B. Iron(III) Complexes			
$[Fe(TPP)(HIm)_2]Cl\cdot$ MeOH	1.989 (8)	1.974 (24)	1.984	8
$[Fe(TPP)(HIm)_2]Cl\cdot H_2O$[d]	1.994 (12)	1.977 (3)	1.988	16
	1.993 (4)	1.964 (3)	1.983	
$[Fe(TPP)(2\text{-MeHIm})_2]^+$	1.971 (4)	2.013 (4)	1.985	14
$[Fe(Prot\ IX)(1\text{-MeIm})_2]$	1.991 (16)	1.977 (16)	1.986	37
$[Fe(TPP)(t\text{-MU})_2]^+\cdot$ 2THF	1.992 (5)	1.983 (4)	1.989	38
$[Fe(TPP)(c\text{-MU})_2]^+\cdot 1.5C_7H_8$[d]	1.997 (1)	1.967 (7)	1.987	38
	1.995 (17)	1.979 (7)	1.990	

[a] The numbers in parentheses are the estimated standard deviations in the least significant digit(s). [b] Values in angstroms. [c] Average Fe–N bond distances for all $[Fe^{II}PL_2]$ complexes = 2.002 and 1.986 Å for all $Fe^{III}PL_2$ species (L = imidazole). [d] Two independent half-molecules with required inversion symmetry.

inversion centers at the iron(II) atom. This required symmetry element leads to several requirements for the molecular structure. First, the iron(II) atom must be centered in the mean plane of the 24-atom core. Second, the axial imidazole ligand planes must be parallel to each other, and third, the porphyrinato cores cannot be significantly nonplanar. Interestingly, $[Fe(TPP)(1\text{-MeIm})_2]$ also has crystallographically required inversion symmetry and hence all conditions also apply to this molecule.

Equatorial bond distances (Fe–N_p) average 2.001 (2) Å in $[Fe(TPP)(1\text{-VinIm})_2]$ and 1.993 (9) Å in $[Fe(TPP)(1\text{-BzlIm})_2]$.[29] Although these equatorial bond distances are consistent with a ferrous low-spin state,[30] there are relatively few $Fe^{II}PL_2$ complexes for comparison (and none where L is an imidazole). There are two bis(pyridine) complexes[31,32] where Fe–N_p = 1.993 (6) or 2.002 (1) Å, a pyrazine complex[33] with Fe–N_p = 2.004 (3) Å, a bis-(piperidine) complex[34] with Fe–N_p = 2.004 (3) Å, and a bis-(tetrahydrothiophene) complex[35] in which Fe–N_p = 1.996 (6) Å.

A quite informative comparison can be made with the series of low-spin bis(imidazole) complexes of iron(III) where the axial Fe–N(Im) bond distances are also considered. Values for these iron(III) complexes and the iron(II) complexes are given in Table V. It is readily seen that the axial bond distances are shorter

Table VI. Bond Lengths (Å) in $[Fe(TPP)(1\text{-VinIm})_2]\cdot CH_2Cl_2$[a]

Fe–N(1)	2.002 (2)	C(m1)–C(21)	1.498 (3)
Fe–N(2)	1.999 (2)	C(m2)–C(a1)′	1.383 (3)
Fe–N(3)	2.004 (2)	C(m2)–C(a4)	1.392 (3)
N(1)–C(a1)	1.381 (2)	C(m2)–C(11)	1.511 (3)
N(1)–C(a2)	1.381 (3)	C(11)–C(12)	1.380 (3)
N(2)–C(a3)	1.380 (3)	C(12)–C(13)	1.397 (3)
N(2)–C(a4)	1.381 (2)	C(13)–C(14)	1.375 (4)
N(3)–C(3)	1.311 (3)	C(14)–C(15)	1.368 (4)
N(3)–C(1)	1.379 (3)	C(15)–C(16)	1.392 (3)
N(4)–C(3)	1.361 (3)	C(16)–C(11)	1.381 (3)
N(4)–C(2)	1.369 (3)	C(21)–C(22)	1.394 (3)
N(4)–C(4)	1.405 (3)	C(22)–C(23)	1.387 (3)
C(a1)–C(b1)	1.439 (3)	C(23)–C(24)	1.368 (4)
C(a2)–C(b2)	1.437 (3)	C(24)–C(25)	1.368 (4)
C(a3)–C(b3)	1.440 (3)	C(25)–C(26)	1.393 (3)
C(a4)–C(b4)	1.443 (3)	C(26)–C(21)	1.377 (3)
C(b1)–C(b2)	1.345 (3)	C(1)–C(2)	1.346 (3)
C(b3)–C(b4)	1.342 (3)	C(4)–C(5)	1.301 (4)
C(m1)–C(a2)	1.396 (3)	C(6)–Cl(1)	1.737 (4)
C(m1)–C(a3)	1.394 (3)		

[a] The numbers in parentheses are the estimated standard deviations in the least significant digit(s). Primed and unprimed symbols denote a pair of atoms related by an inversion center at iron.

Table VII. Bond Angles (deg) in $[Fe(TPP)(1\text{-VinIm})_2]\cdot CH_2Cl_2$[a]

N(2)FeN(1)	89.71 (7)	C(b4)C(b3)C(a3)	107.14 (19)
N(2)FeN(1)′	90.29 (6)	C(b3)C(b4)C(a4)	107.32 (18)
N(2)FeN(3)	93.28 (7)	C(a2)C(m1)C(21)	117.70 (17)
N(1)FeN(3)	88.36 (7)	C(a3)C(m1)C(21)	118.44 (18)
C(a1)N(1)C(a2)	105.42 (16)	C(a3)C(m1)C(a2)	123.84 (19)
C(a1)N(1)Fe	126.85 (13)	C(a4)C(m2)C(11)	117.26 (18)
C(a2)N(1)Fe	127.52 (12)	C(11)C(m2)C(a1)′	118.52 (18)
C(a3)N(2)C(a4)	105.37 (16)	C(a4)C(m2)C(a1)′	124.20 (18)
C(a3)N(2)Fe	127.72 (13)	C(12)C(11)C(16)	118.62 (19)
C(a4)N(2)Fe	126.63 (13)	C(12)C(11)C(m2)	121.17 (19)
C(3)N(3)C(1)	104.50 (18)	C(16)C(11)C(m2)	120.19 (19)
C(3)N(3)Fe	128.34 (14)	C(11)C(12)C(13)	120.66 (22)
C(1)N(3)Fe	126.67 (15)	C(14)C(13)C(12)	119.87 (23)
C(3)N(4)C(2)	105.91 (19)	C(15)C(14)C(13)	119.91 (22)
C(3)N(4)C(4)	125.49 (19)	C(14)C(15)C(16)	120.26 (24)
C(2)N(4)C(4)	128.58 (20)	C(11)C(16)C(15)	120.64 (23)
N(1)C(a1)C(b1)	109.85 (17)	C(26)C(21)C(22)	118.40 (22)
N(1)C(a1)C(m2)′	125.78 (18)	C(22)C(21)C(m1)	119.79 (21)
C(m2)′C(a1)C(b1)	124.35 (18)	C(26)C(21)C(m1)	121.81 (21)
N(1)C(a2)C(b2)	110.25 (17)	C(23)C(22)C(21)	120.29 (25)
N(1)C(a2)C(m1)	125.56 (17)	C(24)C(23)C(22)	120.47 (26)
C(m1)C(a2)C(b2)	124.17 (19)	C(23)C(24)C(25)	119.93 (25)
N(2)C(a3)C(m1)	125.53 (18)	C(24)C(25)C(26)	120.08 (27)
N(2)C(a3)C(b3)	110.22 (17)	C(21)C(26)C(25)	120.83 (25)
C(m1)C(a3)C(b3)	124.18 (19)	C(2)C(1)N(3)	110.51 (21)
N(2)C(a4)C(b4)	109.96 (17)	C(1)C(2)N(4)	106.64 (20)
N(2)C(a4)C(m2)	125.97 (18)	N(3)C(3)N(4)	112.44 (19)
C(m2)C(a4)C(b4)	124.04 (18)	C(5)C(4)N(4)	125.58 (25)
C(b2)C(b1)C(a1)	107.50 (18)	Cl(1)C(6)Cl(1)″	110.3 (3)
C(b1)C(b2)C(a2)	106.96 (18)		

[a] The numbers in parentheses are the estimated standard deviations in the least significant digit(s). Primed and unprimed symbols denote a pair of atoms related by an inversion center at iron. Double primed and unprimed symbols denote a pair of atoms related by the 2-fold axis at C(6).

(29) Here and elsewhere in this paper, the number in parentheses following an averaged value is the root-mean-square deviation of the averaged value.
(30) Scheidt, W. R.; Reed, C. A. *Chem. Rev.* **1981**, *81*, 543–555.
(31) Li, N.; Petricek, V.; Coppens, P.; Landrum, J. *Acta Crystallogr., Sect. C* **1985**, *C41*, 902–906.
(32) Li, N.; Coppens, P.; Landrum, J. *Inorg. Chem.* **1988**, *27*, 482–488.
(33) Walker, F. A.; Reis, D.; Balke, V. L. *J. Am. Chem. Soc.* **1984**, *106*, 6888–6898.
(34) Radonovich, L. J.; Bloom, A.; Hoard, J. L. *J. Am. Chem. Soc.* **1972**, *94*, 2073–2078.
(35) Mashiko, T.; Reed, C. A.; Haller, K. J.; Kastner, M. E.; Scheidt, W. R. *J. Am. Chem. Soc.* **1981**, *103*, 5758–5767.

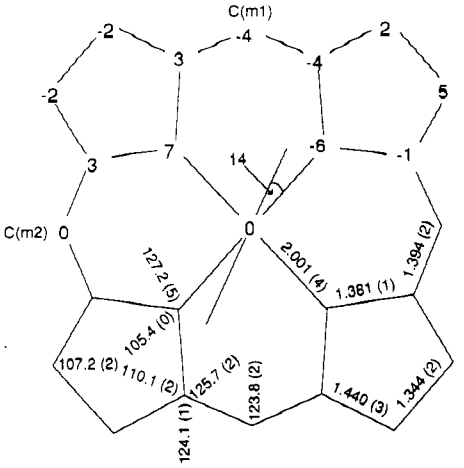

Figure 5. Formal diagram of the porphinato core in the [Fe(TPP)(1-VinIm)$_2$] molecule displaying the averaged values of bond distances and angles in the core. Numbers in parentheses are the root-mean-square deviations from the averaged values. Deviations of each unique atom from the mean plane of the core (in units of 0.01 Å) are shown. Values for the deviations of the centrosymmetrically related atoms have the same magnitude but opposite sign. The orientation of the axial ligand and the angle ϕ are also given.

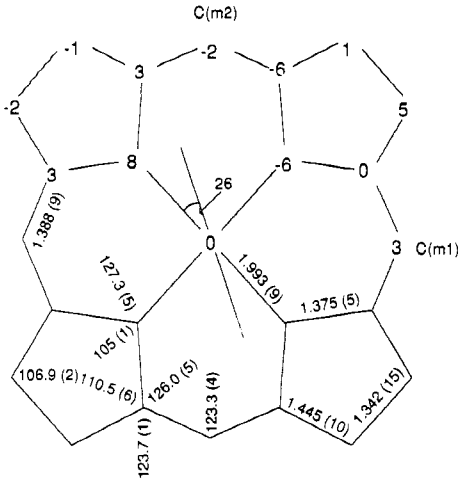

Figure 6. Formal diagram of the porphinato core in the [Fe(TPP)(1-BzlIm)$_2$] molecule. The same information displayed in Figure 5 is given.

in the iron(III) complexes.[36] Interestingly, the average value for the axial and equatorial bonds also allows for a distinction of the oxidation states in bis(imidazole)iron(II, III) complexes. Thus the average value for six Fe–N bonds is 0.016 Å shorter for the low-spin iron(III) complexes than for the low-spin iron(II) species. The data of Table V make clear that this is a consistent difference between all species.

Averaged values for the chemically equivalent bond distances and angles for the two complexes are shown in Figures 5 and 6. Individual values of bond distances and angles including those of the axial ligands are given in Tables VI–IX. Bond distances and angles in both complexes are within normal values and require no additional comment. Figures 5 and 6 also display the deviation of each unique atom, in units of 0.01 Å, from the mean plane of the 24-atom core. Values of the displacements of the centrosymmetrically related atoms have the same magnitude but opposite sign. The core conformations of both species are clearly seen to have a stepped conformation. The core conformation of [Fe(TPP)(1-MeIm)$_2$] is also quite similar. Although the deviations from exact planarity are not large, it is possible that the detailed aspects of these stepped core conformations are related to the axial imidazole tilts and tips (vide infra). Individual units that are expected to be planar, i.e., pyrrole rings, phenyl rings, and imidazole ligands, are indeed all planar to within 0.01 Å.

As we[39] and others[40] have noted, the coordination of imidazoles to metal ions frequently occurs with substantial deviation from

Table VIII. Bond Lengths (Å) in [Fe(TPP)(1-BzlIm)$_2$][a]

Fe–N(1)	1.999 (4)	C(m2)–C(a3)	1.398 (6)
Fe–N(2)	1.986 (4)	C(m2)–C(17)	1.496 (6)
Fe–N(3)	2.017 (4)	C(11)–C(12)	1.387 (7)
N(1)–C(a1)	1.373 (6)	C(12)–C(13)	1.386 (7)
N(1)–C(a2)	1.369 (6)	C(13)–C(14)	1.388 (8)
N(2)–C(a3)	1.380 (6)	C(14)–C(15)	1.377 (8)
N(2)–C(a4)	1.379 (6)	C(15)–C(16)	1.380 (7)
N(3)–C(3)	1.326 (6)	C(16)–C(11)	1.396 (7)
N(3)–C(1)	1.383 (6)	C(17)–C(18)	1.395 (7)
N(4)–C(3)	1.344 (6)	C(18)–C(19)	1.398 (7)
N(4)–C(2)	1.368 (6)	C(19)–C(20)	1.381 (8)
N(4)–C(4)	1.465 (6)	C(20)–C(21)	1.383 (8)
C(a1)–C(b1)	1.450 (6)	C(21)–C(22)	1.390 (7)
C(a2)–C(b2)	1.456 (6)	C(22)–C(17)	1.386 (7)
C(a3)–C(b3)	1.438 (6)	C(1)–C(2)	1.354 (7)
C(a4)–C(b4)	1.436 (6)	C(4)–C(5)	1.513 (7)
C(b1)–C(b2)	1.332 (7)	C(5)–C(6)	1.389 (8)
C(b3)–C(b4)	1.352 (6)	C(6)–C(7)	1.394 (8)
C(m1)–C(a1)	1.384 (6)	C(7)–C(8)	1.389 (9)
C(m1)–C(a4)′	1.404 (6)	C(8)–C(9)	1.374 (9)
C(m1)–C(11)	1.494 (6)	C(9)–C(10)	1.378 (8)
C(m2)–C(a2)	1.382 (6)	C(10)–C(5)	1.388 (7)

[a] The numbers in parentheses are the estimated standard deviations in the least significant digit(s). Primed and unprimed symbols denote a pair of atoms related by an inversion center at iron.

Table IX. Bond Angles (deg) in [Fe(TPP)(1-BzlIm)$_2$][a]

N(2)FeN(1)	89.66 (15)	C(a1)C(m1)C(11)	118.7 (4)
N(2)FeN(1)′	90.34 (15)	C(a4)′C(m1)C(11)	117.1 (4)
N(2)FeN(3)	87.85 (16)	C(a2)C(m2)C(a3)	123.3 (4)
N(1)FeN(3)	93.48 (16)	C(a2)C(m2)C(17)	118.0 (4)
C(a1)N(1)C(a2)	105.8 (4)	C(a3)C(m2)C(17)	118.7 (4)
C(a2)N(1)Fe	127.3 (3)	C(12)C(11)C(16)	117.9 (4)
C(a1)N(1)Fe	126.7 (3)	C(12)C(11)C(m1)	122.4 (4)
C(a4)N(2)C(a3)	104.4 (4)	C(16)C(11)C(m1)	119.6 (4)
C(a3)N(2)Fe	127.8 (3)	C(13)C(12)C(11)	120.7 (5)
C(a4)N(2)Fe	127.4 (3)	C(12)C(13)C(14)	120.6 (5)
C(3)N(3)C(1)	105.3 (4)	C(15)C(14)C(13)	119.1 (4)
C(3)N(3)Fe	123.6 (3)	C(14)C(15)C(16)	120.3 (5)
C(1)N(3)Fe	129.7 (3)	C(15)C(16)C(11)	121.3 (5)
C(3)N(4)C(2)	107.0 (4)	C(22)C(17)C(18)	118.8 (4)
C(3)N(4)C(4)	124.7 (4)	C(22)C(17)C(m2)	121.2 (4)
C(2)N(4)C(4)	127.9 (4)	C(18)C(17)C(m2)	119.9 (4)
N(1)C(a1)C(b1)	110.1 (4)	C(17)C(18)C(19)	120.6 (5)
N(1)C(a1)C(m1)	126.1 (4)	C(20)C(19)C(18)	119.7 (5)
C(m1)C(a1)C(b1)	123.8 (4)	C(19)C(20)C(21)	120.0 (5)
N(1)C(a2)C(b2)	109.9 (4)	C(20)C(21)C(22)	120.2 (5)
N(1)C(a2)C(m2)	126.4 (4)	C(17)C(22)C(21)	120.6 (5)
C(m2)C(a2)C(b2)	123.5 (4)	C(2)C(1)N(3)	109.3 (4)
N(2)C(a3)C(b3)	110.8 (4)	C(1)C(2)N(4)	106.9 (4)
N(2)C(a3)C(m2)	125.4 (4)	N(3)C(3)N(4)	111.5 (4)
C(m2)C(a3)C(b3)	123.8 (4)	N(4)C(4)C(5)	114.1 (4)
N(2)C(a4)C(b4)	111.2 (4)	C(10)C(5)C(6)	118.7 (5)
N(2)C(a4)C(m1)′	125.0 (4)	C(10)C(5)C(4)	118.8 (5)
C(m1)′C(a4)C(b4)	123.7 (4)	C(6)C(5)C(4)	122.4 (4)
C(b2)C(b1)C(a1)	107.1 (4)	C(5)C(6)C(7)	120.5 (5)
C(b1)C(b2)C(a2)	107.2 (4)	C(8)C(7)C(6)	119.4 (5)
C(b4)C(b3)C(a3)	106.9 (4)	C(9)C(8)C(7)	120.3 (5)
C(b3)C(b4)C(a4)	106.6 (4)	C(8)C(9)C(10)	120.0 (5)
C(a1)C(m1)C(a4)′	124.1 (4)	C(9)C(10)C(5)	121.1 (5)

[a] The numbers in parentheses are the estimated standard deviations in the least significant digit(s). Primed and unprimed symbols denote a pair of atoms related by an inversion center at iron.

(36) A possible exception is that of [Fe(TPP)(2-MeHIm)$_2$]$^+$, where the axial imidazoles have a bulky 2-methyl substituent. However the average for the equatorial and axial bond distances fits nicely in the iron(III) series.
(37) Little, R. G.; Dymock, K. R.; Ibers, J. A. *J. Am. Chem. Soc.* **1975**, *97*, 4532–4539.
(38) Quinn, R.; Valentine, J. S.; Byrn, M. P.; Strouse, C. E. *J. Am. Chem. Soc.* **1987**, *109*, 3301–3308.
(39) Momenteau, M.; Scheidt, W. R.; Eigenbrot, C. W.; Reed, C. A. *J. Am. Chem. Soc.* **1988**, *110*, 1207–1215.
(40) Freeman, H. C. *Adv. Protein Chem.* **1967**, *22*, 305–308.

Table X. Imidazole Coordination in Metalloporphyrins[a]

complex	M–N(Im)[b]	DA[c,d]	α[c,e]	β[c,e]	θ[c]	χ[c]	ϕ[c]	$\Delta\phi$[c]	τ[b,f]	ref
[Fe(TPP)(1-VinIm)$_2$]	2.004	77.8	128.3	126.7	3.7	173.5	14	0	0.23	this work
[Fe(TPP)(1-BzlIm)$_2$]	2.017	72.6	123.6	129.7	4.1	169.3	26	0	0.38	this work
[Fe(TPP)(1-MeIm)$_2$]	2.014	88.0	128.2	128.3	1.1	180.2	15	0	0.01	28b
[Fe(TPP)(*c*-MU)$_2$]$^+$[g]	1.967	86.8	125.1	128.9	0.5	177.4	29	0	0.09	38
	1.979	86.0	127.5	126.6	1.0	176.0	15	0	0.14	
[Fe(TPP)(*t*-MU)$_2$]$^+$·2THF	1.983	86.1	127.4	126.5	0.4	177.7	22	0	0.08	38
[Fe(TPP)(HIm)$_2$]Cl·MeOH	1.991	84.0	125.6	127.7	2.2	177.7	18	57	0.08	8
	1.957	85.1	126.2	127.7	178.3	175.4	39		0.16	
[Fe(TPP)(HIm)$_2$]Cl·H$_2$O[g]	1.997	86.4	127.3	127.8	0.6	182.0	6	0	0.07	16
	1.964	87.0	125.7	128.8	0.8	178.2	41	0	0.06	
[Fe(TPP)(2-MeHIm)$_2$]$^+$	2.015	77.9	133.2	120.6	4.3	171.9	32	89.3	0.28	14
	2.010	85.7	132.5	120.5	182.6	176.6	32		0.12	
[Fe(Prot IX)(1-MeIm)$_2$]	1.988	88.3	128.1	127.0	1.4	181.0	3	16	0.03	37
	1.966	89.3	128.8	126.5	181.4	180.8	13		−0.03	

[a] All characters denoted by Greek letters are defined in the text. See also Figure 7 of ref 39. [b] In angstroms. [c] In degrees. [d] DA is the dihedral angle between the ligand plane and the porphinato mean plane. [e] Angles made by the two α-carbons, the axial nitrogen of the imidazole ligand, and iron. [f] Displacement of iron from mean plane of imidazole ligand. [g] Two independent molecules.

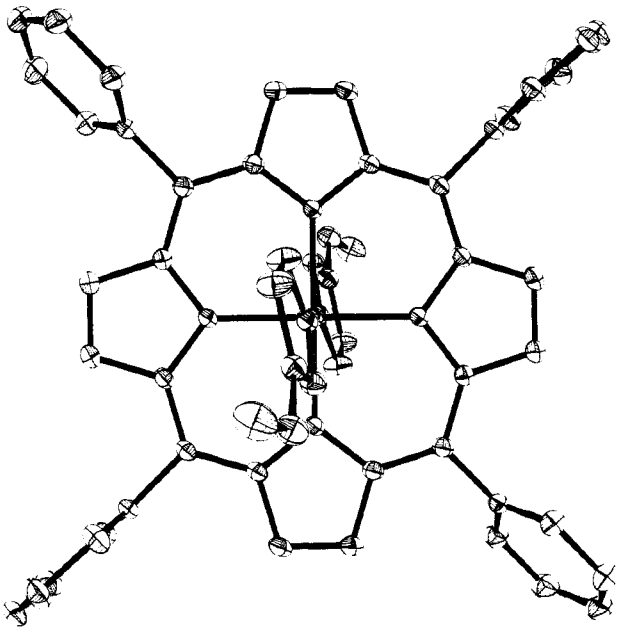

Figure 7. ORTEP diagram of the [Fe(TPP)(1-VinIm)$_2$] molecule showing some conformation aspects of the 1-VinIm ligand and the porphyrin. The view is normal to the porphyrin plane.

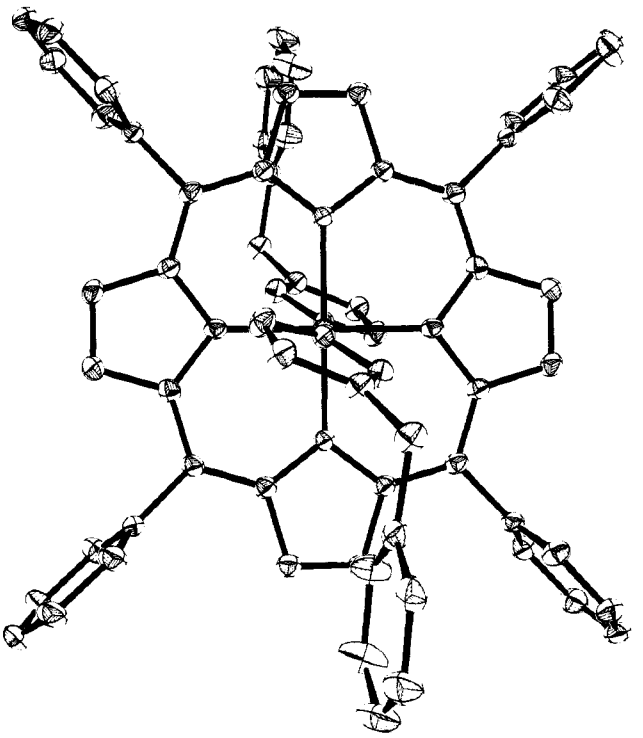

Figure 8. ORTEP diagram of the [Fe(TPP)(1-BzlIm)$_2$] molecule giving the same view as that in Figure 7.

what might be thought of as the "idealized" mode. We have previously defined and tabulated these deviations for metalloporphyrin complexes.[41] These geometrical features are listed in Table X. First is the deviation of the Fe–N(Im) vector from the normal to the N_4 plane, the "tipping" angle θ. Second is the in-plane tilting of the imidazole ligand from the Fe–N(Im) vector, which can be seen in terms of differences in the two Fe–N(Im)–C(α) angles denoted as α and β. The third geometric parameter is the "tilting" of the imidazole ring plane from the Fe–N(Im) vector and denoted by χ. These tipping and tilting parameters can be roughly grouped together as the dihedral angle formed between the porphyrin mean plane and the imidazole plane and listed as DA in Table X. For comparison, we provide the analogous values for several low-spin iron(III) complexes of known structure. As can be seen from the table, the two iron(II) complexes reported herein show larger deviations than the iron(III) complexes, which might be considered to be a general difference between derivatives in the two oxidation states. However the third known iron(II) complex, [Fe(TPP)(1-MeIm)$_2$], does not apparently display such large deviations from ideality.[42] The large deviations from ideality in [Fe(TPP)(1-VinIm)$_2$] and [Fe(TPP)(1-BzlIm)$_2$] can be seen in Figures 7 and 8, which are views down the normal to the heme planes. In both complexes the tilts and tips of the porphyrin core are in the portion of the porphyrin core that leads to the core being further away from the axial ligands.

Discussion

Two important generalizations concerning axial imidazole orientations have been noted.[43,44] These are based on a number of known, detailed bis(imidazole)iron(III) structures as well as other metalloporphyrin imidazole complexes. The first generalization is that small ϕ values are generally preferred for the orientation of an individual ligand. The second generalization is that parallel relative orientations for bis(imidazole) complexes appear to be strongly favored. These preferences continue in the iron(II) species reported herein where all species have parallel ligand orientations and relatively small values ϕ (cf. Table X). Thus the structural data presented herein, along with the [Fe-

(41) See Figure 7 and Tables V and VI of ref 39 for a larger tabulation.
(42) In the [Fe(TPP)(1-MeIm)$_2$] structure, a 2-fold disorder involving the axial ligands may obscure some of the tilts and tips of the imidazole.
(43) Scheidt, W. R.; Chipman, D. M. *J. Am. Chem. Soc.* **1986**, *108*, 1163–1167.
(44) Scheidt, W. R.; Lee, Y. J. Recent Advances in the Stereochemistry of Metallotetrapyrroles. *Struct. Bonding (Berlin)* **1987**, *64*, 1–70.

$(TPP)(1\text{-MeIm})_2$] structure, are most consistent with the bis(imidazole)iron(II) complexes having the same well-developed axial ligand orientation preferences as all other metalloporphyrin species.

Scheidt and Chipman[43] have attempted to define the fundamental electronic reasons for these apparent ligand orientation preferences. They carried out iterative extended Hückel calculations on a number of imidazole-ligated metalloporphyrins as a function of axial ligand orientation angle. From these rotational calculations they suggested that imidazole ligand π donation to metal $p\pi$ and $d\pi$ orbitals leads to the preference for the small ϕ ligand orientations. In the iron(III) systems, in which there are unequally filled metal $d\pi$ orbitals, ligand $p\pi$ to metal $d\pi$ bonding favors the parallel ligand relative orientation. This bonding effect, however, does not explain the parallel relative orientation preference of other bis(imidazole) metalloporphyrin derivatives. The present iron(II) results do not shed further light on this issue. We may note, however, the fact that bis(hindered imidazole)iron(II) complexes cannot be prepared (except perhaps at very low temperatures[45]) is consistent with a strong tendency for parallel ligand orientation. Walker et al.[4] have discussed the possible effects of varying axial ligand orientation on the redox potentials of the $Fe^{II/III}$ couple of cytochromes *b*. They suggested that a perpendicular orientation of the two axial imidazole ligands could yield a more positive redox potential. (However, the effect could yield no more than 50 mV.) The apparently well-developed parallel axial ligand preference in bis(imidazole)iron(II) species demonstrated in this paper is consistent with this possible orientation effect on the redox potential.

Acknowledgment. We thank the National Institutes of Health for support of this research under Grants GM-38401 (W.R.S.) and HL-16860 to George Lang. We thank Prof. J. L. Hoard for giving us the atomic coordinates for the $[Fe(TPP)(1\text{-MeIm})_2]$ structure and allowing us to quote these results.

Supplementary Material Available: Table IS, listing complete crystal data and intensity collection parameters, Tables IIS and IIIS, giving anisotropic thermal parameters and fixed hydrogen atom positions for $[Fe(TPP)(1\text{-VinIm})_2]$, Tables IVS and VS, listing anisotropic thermal parameters and fixed hydrogen atom positions for $[Fe(TPP)(1\text{-BzlIm})_2]$, and Tables VIS and VIIS, giving bond distances and angles for $[Fe(TPP)(1\text{-MeIm})_2]$ (9 pages); listings (×10) of observed and calculated structure amplitudes for $[Fe(TPP)(1\text{-VinIm})_2]$ and $[Fe(TPP)(1\text{-BzlIm})_2]$ (30 pages). Ordering information is given on any current masthead page.

(45) Wang, C.-M.; Brinigar, W. S. *Biochemistry* **1979**, *18*, 4960-4977.

Contribution from the Department of Chemistry, Boston College, Chestnut Hill, Massachusetts 02167-3809

Synthesis and Electrochemistry of Pterins Coordinated to Tetraammineruthenium(II)

Angel Abelleira, Roy D. Galang, and Michael J. Clarke*

Received May 5, 1989

Compounds of the general type *cis*-$[L(NH_3)_4Ru]Br_2$, in which the Ru(II) is coordinated between the N5 and O4 sites, have been synthesized, where L = lumazine, 1,3-dimethyllumazine, 3-methylpterin, 8-methylpterin, and 3,6,7-trimethylpterin. These complexes have been characterized as to their electrochemistry and electronic and fluorescence spectra. Voltammetry and controlled-potential coulometry show that coordinated pterins methylated at N3 undergo a 1e redox process, which is reversible in DMF on the CV time scale. Intense retrodative bonding with Ru(II) raises the potential for the Ru(III,II) couple to the range 560-720 mV and alters the site of protonation to N8.

Owing to the close association of metal ions and pterin coenzymes in many biological redox processes, we have prepared a series of pterin complexes, using Ru(II) to attain a stable metal-pterin bond, to investigate the spectroscopic and electrochemical effects of pterin coordination and show that single-electron transfer is possible for some pteridine ligands when coordinated at the N5 position. Pterin cofactors (derivatives of 2-amino-4(3*H*)-pteridinone) undergo complex redox processes (see Figure 1) and are essential to the function of a number of important metal-containing redox enzymes.[1,2] Examples are (1) the iron-requiring phenylalanine, tyrosine, and tryptophan monooxygenases (2) formate dehydrogenase, which contains W, Se, and Fe,[3] and (3) the molybdenum cofactor (Mo-co), which involves metal coordination of a pterin side chain and occurs in at least ten different enzymes, including nitrate reductase, sulfite oxidase, and xanthine oxidase.[4-7] There is also some evidence that pterins may be involved in photobiological processes.[8]

Phenylalanine 4-monooxygenase requires a 6-substituted tetrahydrobiopterin, which is in close association with an iron center,[9,10] to catalyze the conversion of phenylalanine to tyrosine. This product undergoes a subsequent conversion by tyrosine 3-monooxygenase to dopa (3,4-dihydroxyphenylalanine), a precursor for the neutrotransmitters epinephrine and norepinephrine.[11] In the genetic absence of this enzyme (phenylketonuria), phenylpyruvic acid accumulates in the blood to impair brain development. The quinonoid dihydropterin produced in pterin enzymatic processes is reduced by dihydropterin reductase in the presence of NADPH or NADH back to the tetrahydropterin.[12] The phenylalanine hydroxylase from *Chromobacterium violaceum* appears to involve a type 2 copper center, which may be coordinated to a reduced pterin ring.[13]

The coordination chemistry of pteridines has received relatively little attention. Albert originally investigated complexes of 8-

(1) Coughlan, M. *Molybdenum and Molybdenum Containing Enzymes*; Pergamon Press: New York, 1980.
(2) *Molybdenum Enzymes*; Spiro, T. G., Ed.; Wiley-Interscience: New York, 1985.
(3) Yamamoto, I.; Saiki, T.; Liu, S.-M.; Ljungdahl, L. G. *J. Biol. Chem.* **1983**, *258*, 1826.
(4) Johnson, J. L.; Hainline, B. E.; Rajagopalan, K. V. *J. Biol. Chem.* **1980**, *255*, 1783.
(5) Johnson, J. L.; Rajagopalan, K. V. *Proc. Natl. Acad. Sci. U.S.A.* **1982**, *79*, 6856.
(6) Davis, M. D.; Olson, J. S.; Palmer, G. *J. Biol. Chem.* **1982**, *257*, 14730.
(7) Harlan, E. W.; Berg, J. M.; Holm, R. H. *J. Am. Chem. Soc.* **1986**, *108*, 6992-7000 and references therein.
(8) Chanhidi, C.; Aubailly, M.; Momzikoff, A.; Bazin, M.; Santus, R. *Photochem. Photobiol.* **1981**, *33*, 641.
(9) Dix, T. A.; Bollag, G. E.; Domanico, P. L.; Benkovic, S. J. *Biochemistry* **1985**, *24*, 2955.
(10) Wallick, D. E.; Bloom, L. M.; Gaffney, B. J.; Benkovic, S. J. *Biochemistry* **1984**, *23*, 1295.
(11) (a) Kaufman, S. *J. Biol. Chem.* **1957**, *226*, 511. (b) Kaufman, S. *J. Biol. Chem.* **1958**, *230*, 931. (c) Kaufman, S. *Proc. Natl. Acad. Sci. U.S.A.* **1963**, *50*, 1085. (d) Kaufman, S. *J. Biol. Chem.* **1964**, *239*, 332.
(12) Crane, J. E.; Hall, E. S.; Kaufman, S. *J. Biol. Chem.* **1972**, *247*, 6082.
(13) Pember, S. O.; Benkovic, S. J.; Villagranca, J. J.; Pasenkiewicz-Gierula, M.; Antholine, W. E. *Biochemistry* **1987**, *26*, 4477-83.

0020-1669/90/1329-0633$02.50/0